Accepted Manuscript

Structural, electrical, optical and thermoelectric properties of e-beam evaporated Bi-rich Bi2Te3 thin films

C. Sudarshan, S. Jayakumar, K. Vaideki, Subhajit Nandy, C. Sudakar

PII: S0040-6090(19)30010-0
DOI: https://doi.org/10.1016/j.tsf.2019.01.010
Reference: TSF 37093

To appear in: *Thin Solid Films*

Received date: 20 September 2018
Revised date: 19 December 2018
Accepted date: 9 January 2019

Please cite this article as: C. Sudarshan, S. Jayakumar, K. Vaideki, Subhajit Nandy, C. Sudakar , Structural, electrical, optical and thermoelectric properties of e-beam evaporated Bi-rich Bi2Te3 thin films. Tsf (2019), https://doi.org/10.1016/j.tsf.2019.01.010

This is a PDF file of an unedited manuscript that has been accepted for publication. As a service to our customers we are providing this early version of the manuscript. The manuscript will undergo copyediting, typesetting, and review of the resulting proof before it is published in its final form. Please note that during the production process errors may be discovered which could affect the content, and all legal disclaimers that apply to the journal pertain.

ACCEPTED MANUSCRIPT

Structural, electrical, optical and thermoelectric properties of e-beam evaporated Bi-rich Bi_2Te_3 thin films

C. Sudarshan[a,*] c.sudarshans@gmail.com, S. Jayakumar[b], K. Vaideki[a], Subhajit Nandy[c] and C. Sudakar[c]

[a]Thin Film Centre, Department of Applied Science, PSG College of Technology, Coimbatore 641004, India
[b]Department of Physics, PSG Institute of Technology and Applied Research, Coimbatore 641062, India
[c]Multi-Functional Materials Laboratory, Department of Physics, Indian Institute of Technology Madras, Chennai 600036, India

[*]Corresponding author.

ACCEPTED MANUSCRIPT

ACCEPTED MANUSCRIPT

Abstract

Bi-rich Bi_2Te_3 thin films are prepared at 300 K using e-beam evaporation technique. A source power of 45 W for e-beam was used. Post deposition, these as-deposited Bi-rich Bi_2Te_3 (Bi-BT-AD) films are annealed at 100 °C (Bi-BT-100), 200 °C (Bi-BT-200) and 300 °C (Bi-BT-300) for 1 h under a pressure of 3×10^{-4} Pa. X-ray diffraction measurements reveal the presence of Bi phase together with crystalline Bi_2Te_3 indicating the possible presence of Bi-rich Bi_2Te_3 phase in the Bi-BT-AD film. The broad peaks from Bi_2Te_3 (015) plane indicates nanocrystalline nature of particles. With annealing, no change in diffraction pattern is observed for Bi-BT-100. However, Bi-BT-200 and Bi-BT-300 films show the emergence of x-ray reflection from unknown phases around $2\theta \sim 20°$ and 47°. This indicates Bi related secondary phase segregation and the thermodynamic instability for the presence of Bi in Bi_2Te_3 lattice. From Raman studies it is discerned that Bi secondary phase coexist along with the Bi-rich Bi_2Te_3 nanocrystalline grains. On vacuum annealing Bi-rich Bi_2Te_3 thin films prevails as evidenced from the p-type electrical characteristics, while excess Bi disappears and converts into an unknown minor phase. The resistivity of all the annealed films are $\sim 0.9 \times 10^{-4}$ Ωcm. The Seebeck coefficients also do not show any change and remain around 33 to 36 μV/K. Thermoelectric properties of Bi-BT-100 exhibit high power factors when measured at different ΔT with a maximum of $\sim 17.5 \times 10^{-4}$ W/K^2m for ΔT=100 °C. Thus, unlike the near-stoichiometric thin films, Bi-rich thin films require low temperature annealing (~100 °C) to achieve optimized parameters. Bi-rich Bi_2Te_3 thin films also show higher power factor compared to the near-stoichiometric thin films. Thus, favourable thermoelectric properties can be achieved at 300 K for temperature sensitive device fabrication using Bi-rich Bi_2Te_3 thin films.

Keywords: Bismuth-rich bismuth telluride; thin films; electron-beam evaporation; power factor.

ACCEPTED MANUSCRIPT

1. Introduction

Bismuth telluride (Bi_2Te_3) is one of the most important thermoelectric material used in state-of-the-art devices such as thermoelectric coolers and thermocouples operating in the temperature range between 200 K and 400 K [1, 2]. From the experimental results and theoretical calculation, it has been demonstrated that if the material is in nanostructure form the value of figure of merit is significantly larger [3-10]. In recent years, the attention to develop nanostructured thermoelectric thin film devices has increased with an intent to apply them for diverse applications like micro thermoelectric coolers [11], generators [12] and sensors [13]. For wider range of commercial applications, bismuth telluride based compounds (*p*-type and *n*-type) with high figure of merit and higher thermoelectric conversion efficiency should be explored and developed. The increase in the figure of merit value in low dimensional nanostructured material mainly depend on the carrier mobility improvement due to quantum confinement effect and the reduction of thermal conductivity due to strong phonon scattering in grain boundary [14]. The formation of negatively charged antisite defect (such as Bi_{Te}) in Bi_2Te_3 film, due the excess cation atom occupying the vacant anion sites, leads to the *p*-type conductivity of the film [15-18]. Few studies have been carried out to prepare *p*-type Bi_2Te_3 films. The techniques used include co-evaporation on heated glass substrate [19] and combinatorial sputter coating technology on quartz-single crystal substrates [20]. Fan *et al*. [21] have reported the p-type behaviour in bismuth doped antimony telluride using tri-target co-sputtering deposition technique. Using ion beam sputtering Zheng *et al*.[22] have optimized the preparation of Bi_2Te_3 films at various substrate temperatures to obtain optimal thermoelectric properties. However, *p*-type Bi_2Te_3 thin films prepared using e-beam evaporation technique have not been reported. It is also desirable to prepare *p*-type Bi_2Te_3 thin films on substrates without any annealing process. Such room temperature fabrication of *p*-type Bi_2Te_3 is important for the fabrication of thermoelectric devices over microelectronics. Room temperature deposition ensures the intactness of the microelectronic devices as well as the unaltered *p*-type conductivity of Bi_2Te_3 due to annealing processes.

In this manuscript Bi-rich Bi_2Te_3 thin films are prepared by e-beam evaporation technique. A detailed structural, morphological, optical and electrical property are presented as a function of vacuum annealing temperature. The *p*-type characteristics of Bi_2Te_3 thin films and its

ACCEPTED MANUSCRIPT

influence on the thermoelectric properties are investigated. *p*-type characteristics of Bi_2Te_3 thin films are shown to be favourable compared to the stoichiometric thin films.

2. Experimental Procedure

Bi-rich Bi_2Te_3 thin films are deposited by electron beam (e-beam) evaporation technique. The deposition system from HIND HI-VAC (model: 12A4D) fitted with electron beam power supply (model: EBG-PS-3K) was used. The fluxes of Te and Bi during the e-beam evaporation are altered by controlling the power to the electron gun as detailed in our previous report [23]. A detailed presentation on the control parameters for preparing stoichiometric, Bi and Te-rich Bi_2Te_3 films are reported elsewhere [23]. Near stoichiometric Bi_2Te_3 films were obtained for deposition carried out with a source power of 67.5 W with the substrates positioned at the center of the holder. For obtaining Bi-rich Bi_2Te_3 composition, a source power of 45 W was used. For the current study, the Bi-rich Bi_2Te_3 films were deposited on ultrasonically cleaned glass substrates positioned at the centre of the substrate holder using 45 W source power. These as deposited Bi-rich Bi_2Te_3 films (Bi-BT-AD) were further annealed at 100 °C (Bi-BT-100), 200 °C (Bi-BT-200) and 300 °C (Bi-BT-300) for 1 h under vacuum at a pressure of 3×10^{-4} Pa.

The phase formation of the thin films were examined by a X'pert-pro PANalytical X-ray diffractometer using Cu Kα radiation of λ = 1.5406 Å. The lattice parameters *a* and *c* are estimated from the Rietveld refinement of the experimental X-ray diffraction (XRD) data obtained from the as-deposited and annealed Bi-rich Bi_2Te_3 thin films. Structural files of Bi_2Te_3 (ICDD# 15-0863) and Bi (ICDD# 85-1329) were used as input structural data. The refinements were carried out by allowing the lattice parameter and crystal orientation to be refined. Best fits with $\chi^2 < 2$ were obtained. The surface microstructural details and the thickness of the e-beam deposited films were obtained from the topographic and cross-sectional scanning electron micrographs using FEI Quanta FEG 200/FEG 400 Field Emission Scanning Electron Microscope (FESEM). The composition of the films were estimated from the energy dispersive X-ray spectra (EDS) with an uncertainty of ~0.5 *at.*%. EDS elemental mapping was also carried out to ascertain the spatial homogeneity of the compositions in the films. Bright field transmission electron miscroscopy (TEM) images, high-resolution TEM images, and selected area electron diffraction are obtained using JEOL JEM 2100 High Resolution Transmission Electron

ACCEPTED MANUSCRIPT

Microscope (HRTEM) operating at 200 kV. Atomic force microscopy (AFM) images were obtained in a semi contact mode to analyse the surface topography of thin films using NT-MDT, Russia microscope. Diffuse reflection spectra in IR range (500 to 4000 cm^{-1}) at room temperature are obtained using Perkin Elmer 2 plus spectrometer. Optical bandgap of the films were estimated using Tauc plots. A home-built four probe set up is used to measure resistivity using a Keithley 2400 current source meter. Carrier concentration and mobility are obtained by measuring Hall voltage from ECOPIA (HMS-3000 with B= 0.553 T). Raman spectral studies of Bi-rich Bi_2Te_3 thin film were carried out at 300 K using a Horiba Jobin-Yvon (HR800 UV) micro-Raman spectrometer with a 488 nm excitation line of Ar ion laser. Seebeck coefficient of thin films coated on 7.5 cm long and 1 cm wide glass substrates were measured using a home-built set up. A temperature gradient (ΔT) of ~ 30 °C to ~125 °C was maintained between the hot (varied by a resistive heater) and cold ends (4 °C) of Cu block. The temperature gradient and Seebeck voltage were measured with good thermal and electrical contacts with in a distance of 5 cm. The Seebeck coefficient was obtained by taking the ratio of Seebeck voltage and temperature gradient with a measured uncertainty ~ 5 %. The thermoelectric power factor was calculated using the measured values of Seebeck coefficient and the electrical conductivity.

3. Results and Discussion:

Figure 1(a) shows the XRD pattern of the as-deposited and post annealed Bi-rich Bi_2Te_3 films. The XRD patterns are compared with the powder diffraction pattern files of Bi_2Te_3 (ICDD # 015-0863) and Bi (ICDD # 085-1329) phase. The strong reflections at 2θ~27° and 37° in the diffraction pattern of these two phases overlap significantly. Few distinct peaks (2θ~40° and 41.2°) can be used to differentiate the Bi and Bi_2Te_3 phases. The x-ray reflection of Bi-BT-AD film has a strong reflection at 2θ ~ 27.70°, and 37.82° corresponding to (015) and (10 10) planes. In addition to this, weak reflections from Bi phase are also seen at 2θ ~ 22.35°, 27.08°, 37.93°, 39.66° and 45.91°. These reflections correspond to (003), (012), (104), (110) and (113) planes, respectively, of Bi phase as indexed in Figure 1(a). Thus the presence of Bi phase together with Bi_2Te_3 in the as deposited film indicates the possible presence of Bi-rich Bi_2Te_3 phase. Rietveld refinement on the Bi-BT-AD films also suggested almost 60:40 ratio between Bi_2Te_3 and Bi. In the as-deposited film the crystallinity of the Bi phase is found to be poor. The broad peaks from Bi_2Te_3 (015) plane indicates the presence of nanocrystalline particles

ACCEPTED MANUSCRIPT

in the film. For Bi-BT-100 no significant change in the diffraction pattern is observed. However, films annealed at 200 °C and 300 °C show the emergence of unknown phase around 2θ ~ 20° and 47° (marked with * in Figure 1(a)). It is interesting to note that with annealing the evolution of XRD patterns of the Bi-rich films in comparison to the stoichiometric [23] and Te-rich thin films are very distinct [24]. The presence of unknown secondary phase in 300 °C (Bi-BT-300) annealed thin film indicates the difficulty in pushing Bi into Bi_2Te_3 lattice.

From the Rietveld refinement of as-deposited and annealed Bi-rich Bi_2Te_3 thin films, the lattice parameter *a* and *c* and the particle size are estimated. The changes in the lattice parameter are plotted in Figure 1(b) and the values are shown Table 1. It should be noted that the 300 °C annealed films has poor fitting parameters mainly due to the unknown phase. The variation of these parameters as a function of annealing temperature is shown in Figure 1(b). The estimated lattice parameter of Bi-BT-AD films are a = 4.6020 Å and c = 29.9578 Å. The a-axis parameter is significantly larger than the bulk Bi_2Te_3 value (a = 4.3858 Å) and could be the result of Te atoms (atomic radius = 140 pm) being replaced by larger Bi atoms (atomic radius = 160 pm) [25].

Since Te and Bi atoms form alternate layers of stacks in the Bi_2Te_3 quintuple, the replacement of Bi in the Te plane lead to the enlarged lattice parameter *a*. On annealing the variation of *a* is drastic for Bi-BT-200. These changes imply the Bi being removed from the Bi_2Te_3 lattice and form an unknown secondary phase. With further annealing the changes are found to be small. The lattice parameter *c* is close to the bulk value in the AD film. Annealing at 100°C, 200°C and 300 °C shows a slight decrease in the lattice parameter. The average crystallite size estimated from the refinement of the film shows an increase from 170 Å for as deposited film to 308 Å for the film annealed at 300 °C.

The structure of the nanosized materials at the microscopic level can be inferred using Raman spectroscopy. The observed Raman spectra of Bi-BT-100 films and of the films vacuum annealed at 100°C to 300 °C are shown in Figure 2(a). The magnified region in the range between 50 cm^{-1} and 175 cm^{-1} are shown in Figure 2(b). The frequency and corresponding assignment of Raman peaks in Figure 2(b) are listed in Table 2. The symmetric out of plane

ACCEPTED MANUSCRIPT

vibration mode A_{1g}^{1} of Bi_2Te_3 is observed in the Bi-BT-AD films at wave number ~ 65 cm^{-1}. Such peak never appears prominently in the near stoichiometric [23] and Te-rich Bi_2Te_3 films prepared by e-beam evaporation technique [24]. As the annealing temperature increases to 100 °C this vibrational mode gets suppressed and with further annealing at higher temperatures the intensity remains weak yet distinctly discernible. The reduction in the intensity of A_{1g}^{1} mode with annealing temperature shows that there is a reduction in the interlayer interaction. Additional peaks which are different from the allowed vibrational modes are observed in the Bi-BT-AD films of Bi-rich Bi_2Te_3 films. These modes appearing at ~ 83-87 cm^{-1}, 91-96 cm^{-1} and 97 $cm^{-1}$are denoted as P_1, P_2 and P_3 respectively in Figure 2(b). P_3 is observed only in the as-deposited film, which is mainly caused by the rhombohedral bismuth phase present in the films. Thus the P3 correspond to non-degenerate A_{1g} phonon modes from Bi phase [26]. The peak P_2 ~ 91- 96 cm^{-1} is seen in all the films. This does not correspond to either Bi_2Te_3 or Bi phase. However, such modes have been reported to be due to surface phonon mode, which is only observed in the nanosized materials. The absence of such mode in stoichiometric and Te-rich Bi_2Te_3 thin films despite of the nanocrystalline nature of the crystallites further indicate that the occurrence of this mode becomes prominent due to the significant increase in the interatomic distances from the surface layers compared to the bulk samples [27].

The large lattice parameter a due to Bi-rich Bi_2Te_3 also suggests that these modes could be prominent only when the interatomic distances become large due to the insertion of large cations like Bi in the lattice. On annealing the frequency of this mode changes from ~91 cm^{-1} for as-deposited film to ~ 96 cm^{-1} for the film annealed at 200 °C (blue shifts) and reduces to ~92 cm^{-1} for the film annealed at 300 °C compared to as-deposited films. The large intensity of P_2 compared to other modes implying a strong surface phonon interaction between layers may lead to an increase in thermal conductivity thus reducing the figure of merit. The origin of P_1 is unknown and probably arises from the unknown secondary phases observed in XRD pattern [28].

The surface morphology and cross sectional micrographs of as-deposited and annealed Bi-rich Bi_2Te_3 thin films are recorded using FESEM (Figure 3). The surface of as-deposited film overall appears uniform and smooth. Few patchy regions of different roughness are seen with dark contrast in the AD and 100 °C annealed samples (refer to Figure 3(a) and 3(b)). Such

ACCEPTED MANUSCRIPT

features are not seen in the 200 °C and 300°C annealed thin films. These regions could be due to Bi rich composition. For all the films, formation of few protrusions with white contrast are also seen. Such cluster like protrusion were seen in the stoichiometric and Te-rich thin film surfaces as well [24]. As the annealing temperature increases the size of the grains increase and the grains become more densely packed [29]. The changes also result in surface roughness variation. Detailed study using AFM are presented in the following section. From the cross sectional SEM images, thickness of as-deposited and annealed films are estimated. All the films have uniform thickness of ~ 250 nm (Table 3 and Figure 3). The annelaing process of as-deposited thin films do not show any thickness variation. The Bi and Te EDS elemental mapping for the Bi-rich Bi_2Te_3 thin films are shown in Figure 4 along with the topographic regions from where the mappings were recorded. The morphology and spatial elemental distribution suggest that there is no discernible segregation of Bi-rich regions. The films look compositionally uniform at all annealing conditions. Though the e-beam probe size is ~ 5 nm, the interaction volume of the e-beam in the samples could be several hundreds of nm^3 below the surface. Thus, we could conclude that large inhomogeneous Bi-rich segregations are not seen in any of these thin films. The Bi-rich regions could be very local with the size in the range of few nanometer. The average EDS spectra obtained from these regions are shown in the spectra provided in Figure 4. The composition of the films were estimated from EDS spectra and the values are tabulated in Table 3. The estimated values show that all the films have Bi:Te ratio of 50:50 confirming the bismuth rich composition in the films (Table 3).

The AFM images of Bi-rich Bi_2Te_3 film surfaces are shown in Figure 5 (a to d). In the as-deposited film, the grain distribution is very uniform all over the surface. The average roughness of these films is 3.6 nm. The film annealed at 100 °C shows vertically standing islands of grains with size ~ 10 to 20 nm. On annealing the density of this grains seem to increase. The annealing at 100 °C seems to drastically increase the roughness to 5.3 nm (Table 3). Vacuum annealing at higher temperatures (200 °C and 300 °C) bring the roughness below 3 nm. Excess Bi present in the AD films reacting with Bi_2Te_3 and the formation of unknown phase could alter the roughness on annealing.

To determine the particle size and phase distribution of Bi-rich Bi_2Te_3 samples TEM studies were carried out. The bright field TEM images of as-deposited and annealed films are

ACCEPTED MANUSCRIPT

shown in Figure 6(a-d) and the corresponding selected area electron diffraction (SAED) images are shown in Figure 6(e-h). The nanocrystalline particles are clearly seen in all the images. The crystallite sizes estimated from the images are in the range between 20 and 30 nm. Even the as-deposited thin film exhibit nanocrystalline nature as seen from the SAED and HRTEM images (Figure 6 and Figure 7). The spotted diffraction rings exactly match with the simulated pattern confirming the Bi_2Te_3 phase formation. Bi phase seen in XRD is not clearly discernible in SAED pattern due to the low scattering. However, the surface regions show some amorphous to poorly crystalline phase as shown by white encircled region in Figure 7a. The annealing of samples does not show any changes in the crystallite size or the phase. The average size remains in the range between 20 to 30 nm. The crystallites exhibit nearly defect free lattice structure as shown in the HRTEM lattice images. The major phase, i.e. rhombohedral structure, is found to be same in all the films. The unidentified phase observed by way of broad low intense peak in the XRD pattern is not identifiable from the TEM analysis.

Bi_2Te_3 has double valence and double conduction band with direct and indirect band gap values [30, 31]. To obtain the bandgap values the diffuse reflection is measured. The obtained diffuse reflections of all the films are shown in Figure 8(a). The absorption coefficient is obtained by converting the diffuse reflection data to Kubelka-Munk function F(R). The direct bandgap values are obtained by plotting $[F(R)h\nu]^2$ vs $h\nu$ as shown in Figure 8(b). The direct band gap shows a linear decrease in E_g from 0.104 eV for as-deposited to 0.099 eV for film annealed at 300 °C except for an initial increase of 0.126 eV for the film annealed at 100 °C. All these values are close to the bulk Bi_2Te_3 theoretical bandgap energy value of ~ 0.11 eV [32, 33]. The small variation found in the bandgap value is due to the microstructural variation as seen in XRD and Raman results during the annealing process in Bi_2Te_3 films. From the plot $[F(R)h\nu]^{1/2}$ vs $h\nu$ shown in Figure 8(c) a clean extrapolation of the curve to the abscissa could not be done. Therefore the result suggests that all the films do not have indirect bandgap [34].

The carrier concentration and mobility of the as-deposited and annealed films are determined at room temperature. These results are presented in Figure 9. All the films show positive Hall coefficient value affirming that the films are *p*-type. The hole carrier concentration of Bi-BT-AD film is 4.29×10^{21} cm^{-3}. With annealing the hole concentration reduces slightly and ranges between 1.2×10^{21} cm^{-3} and 2.4×10^{21} cm^{-3}. Slight variation in the hole concentration

ACCEPTED MANUSCRIPT

values could be due to microstructural variation in the film. The carrier concentrations of all the films are two orders higher than the values reported by Zou et al. [19]. *p*-type semiconductivity in Bi_2Te_3 has been attributed to the excess bismuth atoms accommodating the Te sites in the Bi_2Te_3 lattice forming the anti-site defects, interstitial Bi atom and creation of vacancy on a Te sub-lattice [35]. Out of these Bi_{Te} antisite defects are expected to play a significant role as detailed by Hashibon et al [35]. The mobility of these film ranges between 10 and 30 cm^2/Vs.

The transport properties of as-deposited and vacuum annealed films as a function of temperature were measured and shown in Figure 10. The electrical resistivity decreases with increasing temperature for as-deposited and 100 °C annealed films indicating semiconducting behaviour. On the other hand the films annealed at 200 °C and 300 °C show initial increase in resistivity up to 350 K indicating metallic behaviour. On further heating the resistivity shows no appreciable change and exhibits semiconductive behaviour. Such switching from metallic to semiconductive behaviour could possibly be due to the appearance of unknown phase at high temperature annealing. Metallic characteristics arising from the non-degenerate charge carrier transport through impurity bands are known in the literature for doped Bi_2Te_3 [36, 37]. The activation energy was estimated for the as-deposited and annealed films in a semiconductor region using the relation, $\ln(\sigma) = \ln(\sigma_0) - (E_a/K_BT)$, where σ_0 is the temperature independent conductivity, E_a is the activation energy in joules, K_B is Boltzmann constant and T is absolute temperature. The activation energy varies from 0.031 eV to 0.028 eV for the films annealed ≤ 200 °C. The activation energy is found to be similar to that obtained for Te-rich Bi_2Te_3.

The Seebeck coefficient, resistivity and power factor of as-deposited and annealed Bi-rich Bi_2Te_3 films at room temperature are shown in Figure 11. The positive value of Seebeck coefficient of all the films confirms the *p*-type characteristics. The resistivity of all annealed films are ~ $0.9 \times 10^{-4}\,\Omega$cm. There is no variation in the Seebeck coefficient value i.e. 33 μV/K, for Bi-BT-AD and Bi-BT-100. On further annealing there is a linear increase and reaches a maximum of ~ 36 μV/K for Bi-BT-300. The power factor is calculated using the relation S^2/ρ, where S is Seebeck coefficient and ρ is electrical resistivity. The power factor value ranges between ~$11 \times 10^{-4}\, W/K^2m$ and ~$15\times 10^{-4}\, W/K^2m$. The trend seems to increase with the annealing temperature. The power factor values are close to the results reported by Zou et al [19].

ACCEPTED MANUSCRIPT

The power factor is estimated by measuring the Seebeck coefficient at high temperature gradients (ΔT) as well. The Seebeck coefficient values for all the films shows an increasing trend with applied temperature (Figure 12a) and the maximum value is 44×10^{-4} μV/K for the Bi-BT-200 film. The power factor for all annealed films show a steady increasing trend with ΔT (measured between 30 °C and ~125 °C (Figure 12b). At ΔT = 30 °C, the power factor mostly ranged between 10 and 12×10^{-4} W/K^{2}m. With increasing ΔT a steady increase of 4% per °C is observed. A maximum value ~ 17.5×10^{-4} W/K^{2}m is observed for the film annealed at 100 °C at high temperature gradient (ΔT =100 °C). Studies of thermoelectric properties of Bi-rich Bi_2Te_3 films are very few in the literature [19, 38]. The results of our work show higher power factor values than those reported suggesting that the thin films prepared using the e-beam evaporation method are more suitable for thermoelectric application. We also compare the thermoelectric properties of stoichiometric and Te-rich n-type Bi_2Te_3 thin films along with the Bi-rich p-type Bi_2Te_3 thin films as summarised in Figure 13(a-c). The plots show the effect of vacuum annealing temperature on resistivity, Seebeck coefficient and power factor of near stoichiometric, Te-rich and Bi-rich Bi_2Te_3 films. The Table 4 compares the electrical properties of stoichiometric, Te-rich and Bi-rich Bi_2Te_3 films obtained under optimized annealing condition thus providing the best thermoelectric properties. We find that the power factor, one of the important decider for the choice of thermoelectric material is better for Bi-rich Bi_2Te_3 for as-deposited thin films. Te-rich films Bi-rich Bi_2Te_3 exhibit almost two times less power factor when annealed between 100 and 200 °C. These studies suggest that Bi-rich compositions of Bi_2Te_3 are suitable to be considered as thermoelectric material for ambient deposition conditions.

4. Conclusion

Bi-rich Bi_2Te_3 thin films are prepared at room temperature using e-beam evaporation technique. From XRD, EDS and Raman studies it is discerned that Bi secondary phase coexist along with the Bi-rich Bi_2Te_3 nanocrystalline grains. On vacuum annealing, the Bi-rich Bi_2Te_3 thin films prevail, while excess Bi disappears and converts into an unknown minor phase. The resistivity of all annealed films are found to be ~ 0.9×10^{-4} Ωm. The Seebeck coefficient of the as-deposited and annealed film lies around 33 to 36 μV/K. The effect of applied temperature on

ACCEPTED MANUSCRIPT

thermoelectric properties suggest that the samples annealed at a temperature of 100 °C exhibit high power factor of ~ 17.5 x 10^{-4} W/K^2m and are favourable for thermoelectric applications. Thus, unlike the near-stoichiometric and Te-rich Bi_2Te_3 thin films, Bi-rich thin films require low temperature annealing (~100 °C) to acquire desirable properties. Further, Bi-rich Bi_2Te_3 thin films show higher power factor compared to the near-stoichiometric thin films.

ACCEPTED MANUSCRIPT

ACCEPTED MANUSCRIPT

References

[1] A.F. Ioffe, Semiconductors Thermoelements and Thermoelectric Cooling, Interscience, New York, 1961.

[2] D.M. Rowe, C.M. Bhandari, Modern thermoelectrics, Reston Pub. Co., Reston, Va., 1983.

[3] L.D. Hicks, M.S. Dresselhaus, Effect of quantum-well structures on the thermoelectric figure of merit, Physical Review B, 47 (1993) 12727-12731.

[4] G. Chen, Thermal conductivity and ballistic-phonon transport in the cross-plane direction of superlattices, Physical Review B, 57 (1998) 14958-14973.

[5] D.A. Broido, T.L. Reinecke, Thermoelectric power factor in superlattice systems, Applied Physics Letters, 77 (2000) 705-707.

[6] R. Venkatasubramanian, E. Siivola, T. Colpitts, B. O'Quinn, Thin-film thermoelectric devices with high room-temperature figures of merit, Nature, 413 (2001) 597-602.

[7] D.G. Cahill, W.K. Ford, K.E. Goodson, G.D. Mahan, A. Majumdar, H.J. Maris, R. Merlin, S.R. Phillpot, Nanoscale thermal transport, Journal of Applied Physics, 93 (2003) 793-818.

[8] G. Chen, Diffusion–transmission interface condition for electron and phonon transport, Applied Physics Letters, 82 (2003) 991-993.

[9] D. Vashaee, A. Shakouri, Electronic and thermoelectric transport in semiconductor and metallic superlattices, Journal of Applied Physics, 95 (2004) 1233-1245.

[10] R. Yang, G. Chen, Thermal conductivity modeling of periodic two-dimensional nanocomposites, Physical Review B, 69 (2004) 195316.

[11] L.W. da Silva, M. Kaviany, Micro-thermoelectric cooler: interfacial effects on thermal and electrical transport, International Journal of Heat and Mass Transfer, 47 (2004) 2417-2435.

[12] W. Glatz, E. Schwyter, L. Durrer, C. Hierold, Bi_2Te_3-Based Flexible Micro Thermoelectric Generator With Optimized Design, Journal of Microelectromechanical Systems, 18 (2009) 763-772.

[13] U. Dillner, E. Kessler, H.G. Meyer, Figures of merit of thermoelectric and bolometric thermal radiation sensors, J. Sens. Sens. Syst., 2 (2013) 85-94.

[14] Z.-G. Chen, G. Han, L. Yang, L. Cheng, J. Zou, Nanostructured thermoelectric materials: Current research and future challenge, Progress in Natural Science: Materials International, 22 (2012) 535-549.

[15] Z. Starý, J. Horák, M. Stordeur, M. Stölzer, Antisite defects in $Sb_{2-x}Bi_xTe_3$ mixed crystals, Journal of Physics and Chemistry of Solids, 49 (1988) 29-34.

[16] S. Jia, H. Ji, E. Climent-Pascual, M.K. Fuccillo, M.E. Charles, J. Xiong, N.P. Ong, R.J. Cava, Low-carrier-concentration crystals of the topological insulator Bi_2Te_2Se, Physical Review B, 84 (2011) 235206.

[17] M.K. Fuccillo, S. Jia, M.E. Charles, R.J. Cava, Thermoelectric Properties of Bi_2Te_2Se Compensated by Native Defects and Sn Doping, Journal of Electronic Materials, 42 (2013) 1246-1253.

ACCEPTED MANUSCRIPT

[18] H. Fang, J.-H. Bahk, T. Feng, Z. Cheng, A.M.S. Mohammed, X. Wang, X. Ruan, A. Shakouri, Y. Wu, Thermoelectric properties of solution-synthesized n-type Bi_2Te_3 nanocomposites modulated by Se: An experimental and theoretical study, Nano Research, 9 (2016) 117-127.

[19] H. Zou, D.M. Rowe, G. Min, Growth of p- and n-type bismuth telluride thin films by co-evaporation, Journal of Crystal Growth, 222 (2001) 82-87.

[20] M. Goto, M. Sasaki, Y. Xu, T. Zhan, Y. Isoda, Y. Shinohara, Control of p-type and n-type thermoelectric properties of bismuth telluride thin films by combinatorial sputter coating technology, Applied Surface Science, 407 (2017) 405-411.

[21] P. Fan, T. Chen, Z. Zheng, D. Zhang, X. Cai, Z. Cai, Y. Huang, The influence of Bi doping in the thermoelectric properties of co-sputtering deposited bismuth antimony telluride thin films, Materials Research Bulletin, 48 (2013) 333-336.

[22] Z.H. Zheng, P. Fan, T.B. Chen, Z.K. Cai, P.J. Liu, G.X. Liang, D.P. Zhang, X.M. Cai, Optimization in fabricating bismuth telluride thin films by ion beam sputtering deposition, Thin Solid Films, 520 (2012) 5245-5248.

[23] C. Sudarshan, S. Jayakumar, K. Vaideki, C. Sudakar, Effect of vacuum annealing on structural, electrical and thermal properties of e-beam evaporated Bi_2Te_3 thin films, Thin Solid Films, 629 (2017) 28-38.

[24] C. Sudarshan, Preparation and characterization of Bi_2Te_3 thin films by e-beam evaporation technique for thermoelectric applications (Doctoral dissertation), Anna University, Chennai, 2018.

[25] J.R. Wiese, L. Muldawer, Lattice constants of Bi_2Te_3-Bi_2Se_3 solid solution alloys, Journal of Physics and Chemistry of Solids, 15 (1960) 13-16.

[26] J.A. Steele, R.A. Lewis, In situ micro-Raman studies of laser-induced bismuth oxidation reveals metastability of β-Bi_2O_3 microislands, Opt. Mater. Express, 4 (2014) 2133-2142.

[27] C. Wang, X. Zhu, L. Nilsson, J. Wen, G. Wang, X. Shan, Q. Zhang, S. Zhang, J. Jia, Q. Xue, In situ Raman spectroscopy of topological insulator Bi_2Te_3 films with varying thickness, Nano Research, 6 (2013) 688-692.

[28] H. Xu, Y. Song, Q. Gong, W. Pan, X. Wu, S. Wang, Raman spectroscopy of epitaxial topological insulator Bi_2Te_3 thin films on GaN substrates, Modern Physics Letters B, 29 (2015) 1550075.

[29] J. Song, X. Chen, Y. Tang, Q. Yao, L. Chen, Post-annealing Effect on Microstructures and Thermoelectric Properties of $Bi_{0.45}Sb_{1.55}Te_3$ Thin Films Depositedby Co-sputtering, Journal of Electronic Materials, 41 (2012) 3068-3072.

[30] I.G. Austin, The Optical Properties of Bismuth Telluride, Proceedings of the Physical Society, 72 (1958) 545.

[31] H. Rui, W. Zhenhua, L.J.Q. Richard, D. Conor, B. Ben, T.E. Kidd, C.C. Chancey, P.A.G. Xuan, Observation of infrared-active modes in Raman scattering from topological insulator nanoplates, Nanotechnology, 23 (2012) 455703.

ACCEPTED MANUSCRIPT

[32] S.K. Mishra, S. Satpathy, O. Jepsen, Electronic structure and thermoelectric properties of bismuth telluride and bismuth selenide, Journal of Physics: Condensed Matter, 9 (1997) 461.

[33] E.H. Kaddouri, T. Maurice, X. Gratens, S. Charar, S. Benet, A. Mefleh, J.C. Tedenac, B. Liautard, Optical Properties of Bismuth Telluride Thin Films, Bi_2Te_3/Si(100) and Bi_2Te_3/SiO_2/Si(100), physica status solidi (a), 176 (1999) 1071-1076.

[34] Y. Saito, P. Fons, K. Makino, K.V. Mitrofanov, F. Uesugi, M. Takeguchi, A.V. Kolobov, J. Tominaga, Compositional tuning in sputter-grown highly-oriented Bi-Te films and their optical and electronic structures, Nanoscale, 9 (2017) 15115-15121.

[35] A. Hashibon, C. Elsässer, First-principles density functional theory study of native point defects in Bi_2Te_3, Physical Review B, 84 (2011) 144117.

[36] H.J. Goldsmid, Heat Conduction in Bismuth Telluride, Proceedings of the Physical Society, 72 (1958) 17.

[37] A.A. Nadir, M.A. Nadir, V.A. Xayala, G. Samir Sh, G.K. Taira, M.M. Konul, A.N. Sergey, N.Z. Vladimir, Metal–Insulator Transition Induced by Temperature in $Bi_2Te_{3-x}Cl_x$ Layered Compound, Japanese Journal of Applied Physics, 50 (2011) 05FD04.

[38] D.-H. Kim, G.-H. Lee, Effect of rapid thermal annealing on thermoelectric properties of bismuth telluride films grown by co-sputtering, Materials Science and Engineering: B, 131 (2006) 106-110.

ACCEPTED MANUSCRIPT

ACCEPTED MANUSCRIPT

Table 1: Crystallite size, microstrain and structural lattice parameters estimated from the Rietveld refinement of the x-ray diffraction patterns of Bi-rich Bi_2Te_3 thin films annealed for 60 min in vacuum (3×10^{-4} Pa). Estimated standard deviations are given in parentheses.

Bi-rich Bi_2Te_3 thin film	Crystallite size (d±10Å)	Micro strain (%)	Lattice parameter		
			a (Å)	c (Å)	c/a
Bi-BT-AD	170	0.117	4.6020(8)	29.9578(3)	6.5091
Bi-BT-100	178	0.088	4.5956(3)	29.0099(6)	6.3125
Bi-BT-200	190	0.063	4.3062(1)	29.2288(3)	6.7876
Bi-BT-300	308	0.019	4.5197(3)	29.5364(6)	6.5350

Table 2: Peak positions of Raman modes in the as-deposited and annealed Bi-rich Bi_2Te_3 thin films.

Bi-rich Bi_2Te_3 thin film	A^1_{1g} (cm^{-1})	P_1(cm^{-1})	P_2 (cm^{-1})	P_3 (cm^{-1})
Bi-BT-AD	65.48	-	91.26	97.59
Bi-BT-100	-	83.57	93.53	-
Bi-BT-200	65.24	86.51	96.01	-
Bi-BT-300	64.53	87.32	92.60	-

Table 3: Composition from EDS, thickness from cross-sectional SEM, roughness from AFM and bandgap estimation from DRS studies of as deposited and annealed Bi-rich Bi_2Te_3 thin films.

Bi-rich Bi_2Te_3 thin film	*at.* % (± 0.5 %)		Thickness (± 5 nm)	Average Roughness (± 0.1 nm)	RMS Roughness (± 0.1 nm)	Direct Bandgap (± 0.004 eV)
	Bi	Te				
Bi-BT-AD	48.6	51.4	245	3.6	4.4	0.104
Bi-BT-100	51.7	48.3	250	4.1	5.3	0.126
Bi-BT-200	52.6	47.4	250	2.6	3.3	0.101

ACCEPTED MANUSCRIPT

Bi-BT-300	52.3	47.7	250	3.0	3.9	0.099

ACCEPTED MANUSCRIPT

ACCEPTED MANUSCRIPT

Table 4: Comparison of electric properties for Bi_2Te_3 samples exhibiting best thermoelectric properties.

Bi_2Te_3 Sample	**Semiconductor type**	**Optimized vacuum annealing temperature (°C)**	**Carrier concentration (cm^{-3})**	**Resistivity (10^{-4} Ω cm)**	**Seebeck coefficient (μV/K)**	**Power Factor (10^{-4} W/K^2 m)**	**e-beam source power (W)**	**Reference**
Near - stoichiometric	n-type	200	4.04×10^{21}	0.77	-19.5	4.95	67.5	[20]
Te-rich	n-type	200	4.57×10^{21}	3.59	-96.8	27.21	90.0	[21] Also see Fig. 13
Bi-rich	p-type	100	1.18×10^{21}	0.73	30.0	12.32	45.0	This work

ACCEPTED MANUSCRIPT

ACCEPTED MANUSCRIPT

Figure 1: (a) X-ray diffraction patterns of as-deposited and vacuum-annealed Bi-rich Bi_2Te_3 films. Rietveld refinements of the XRD data are also shown in the plots. The measured intensities and the Rietveld patterns are shown in black and red colour lines, respectively. (b) Lattice parameter *a*, *c* and *c/a* ratio of as-deposited and the vacuum annealed Bi-rich Bi_2Te_3 films are shown as a function of annealing temperature.

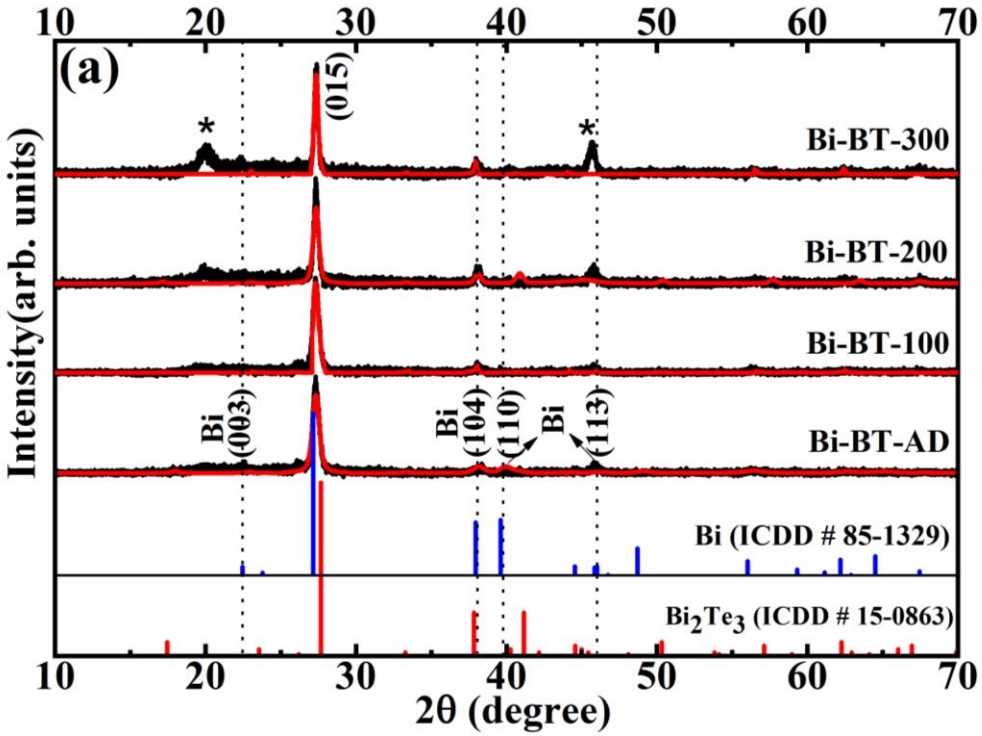

ACCEPTED

ACCEPTED MANUSCRIPT

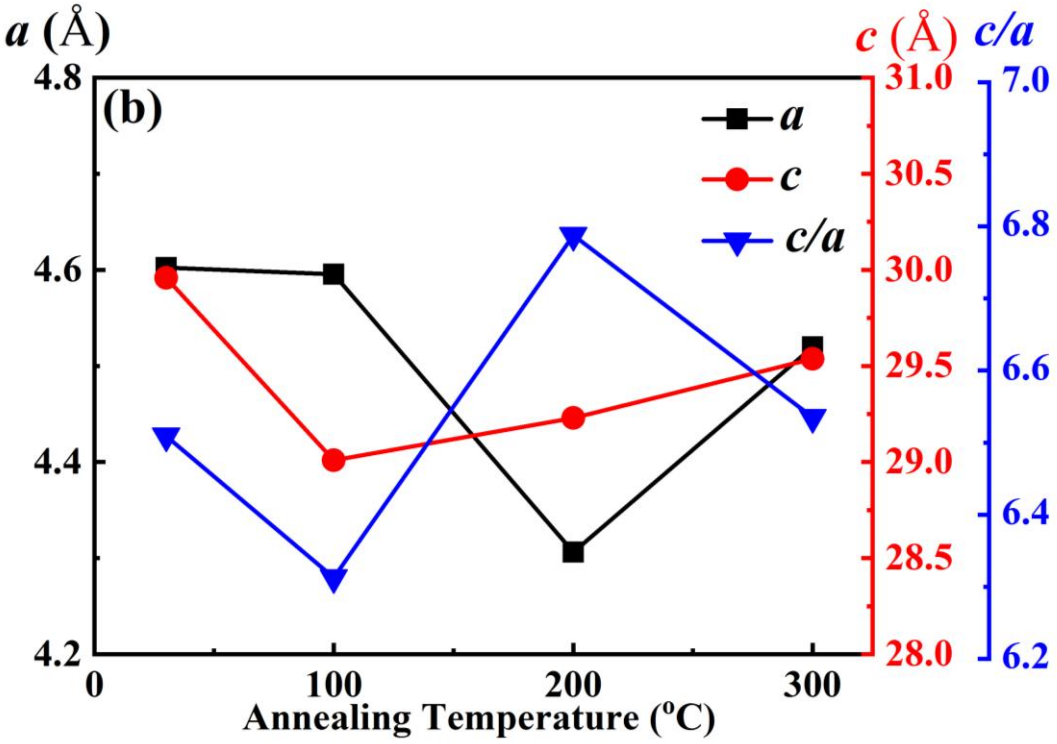

Figure 2: Raman spectra acquired with an excited laser source of wavelength 488 nm on as-deposited Bi-rich Bi_2Te_3 and vacuum annealed thin film at different temperatures. Spectra with (a) Raman shift in the range of 50 cm^{-1} to 1000 cm^{-1} and (b) Raman shift in the magnified region between 50 cm^{-1} to 175 cm^{-1} are shown.

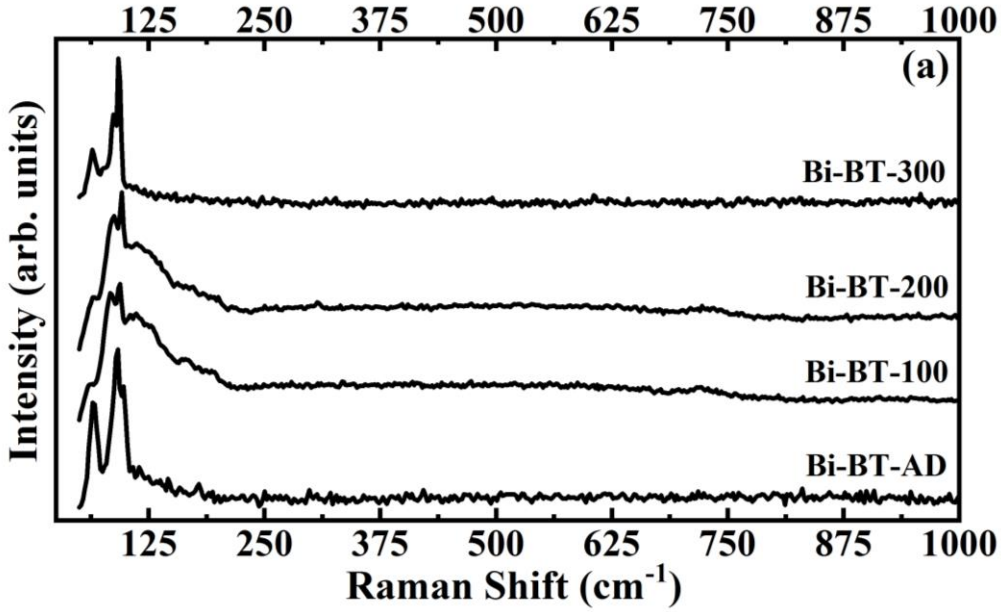

ACCEPTED MANUSCRIPT

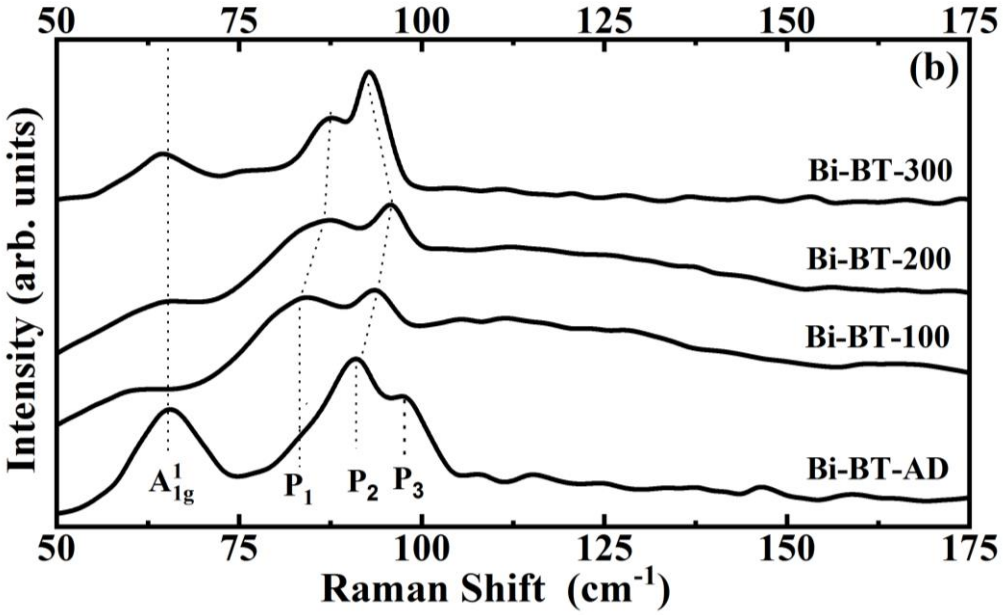

Figure 3: FESEM morphology and cross sectional images of as-deposited and vacuum annealed Bi-rich Bi_2Te_3 thin films at different temperatures: (a, e) Bi-BT-AD; (b, f) Bi-BT-100; (c, g) Bi-BT-200; (d, h) Bi-BT-300.

ACCEPTED MANUSCRIPT

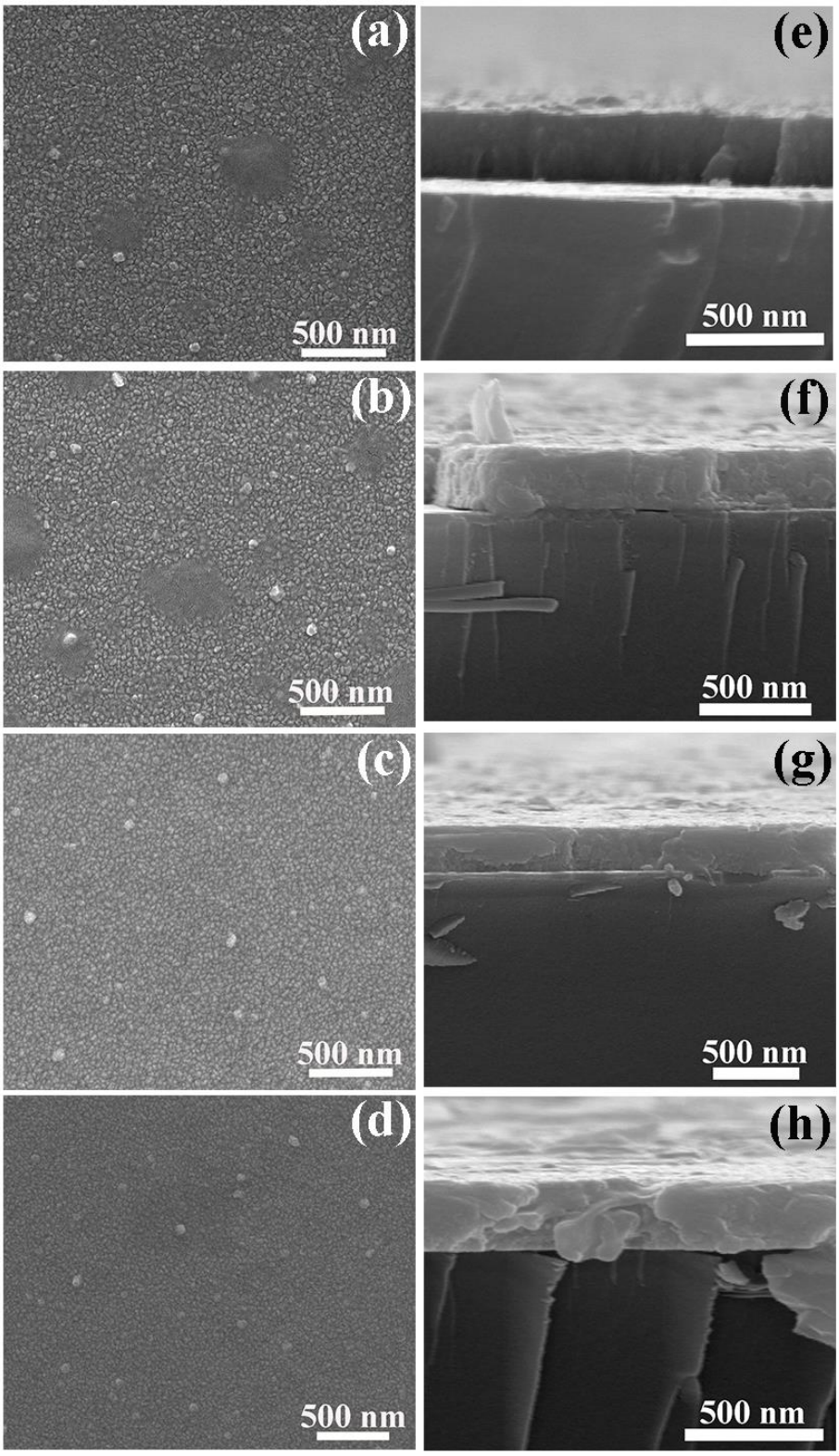

Figure 4: FESEM and EDS results of (a-d) Bi-BT-AD, (e-h) Bi-BT-100, (i-l) Bi-BT-200 and (m-p) Bi-BT-300 thin films. FESEM topography (a, e, i, m), and Bi (b, f, j, n) and Te (c, g, k, o) EDS mapping, and the average EDS spectra (d, h, l, p) are shown.

ACCEPTED MANUSCRIPT

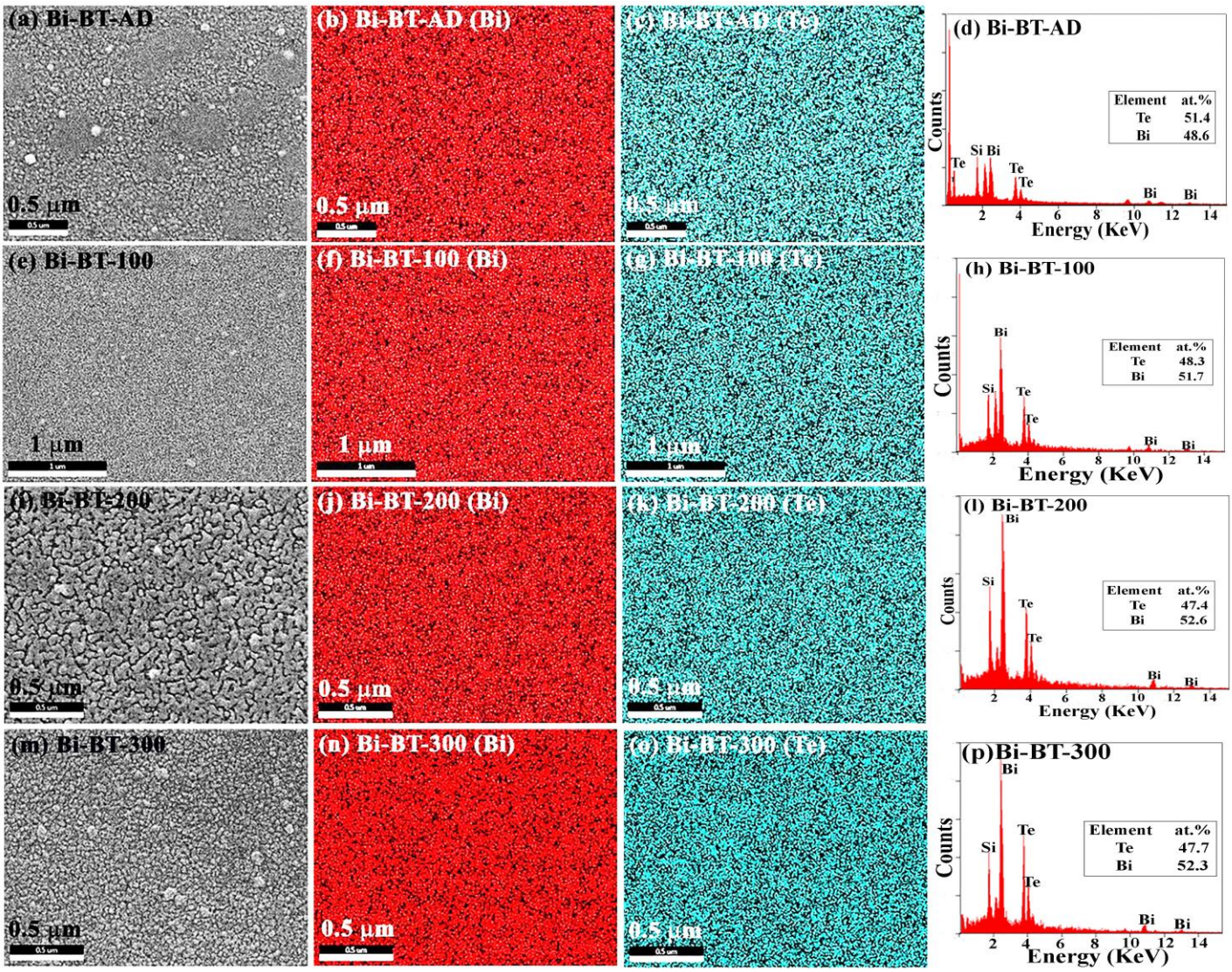

Figure 5: AFM images of as-deposited and vacuum annealed Bi-rich Bi_2Te_3 films at different temperatures: (a) Bi-BT-AD, (b) Bi-BT-100, (c) Bi-BT-200 and (d) Bi-BT-300.

ACCEPTED MANUSCRIPT

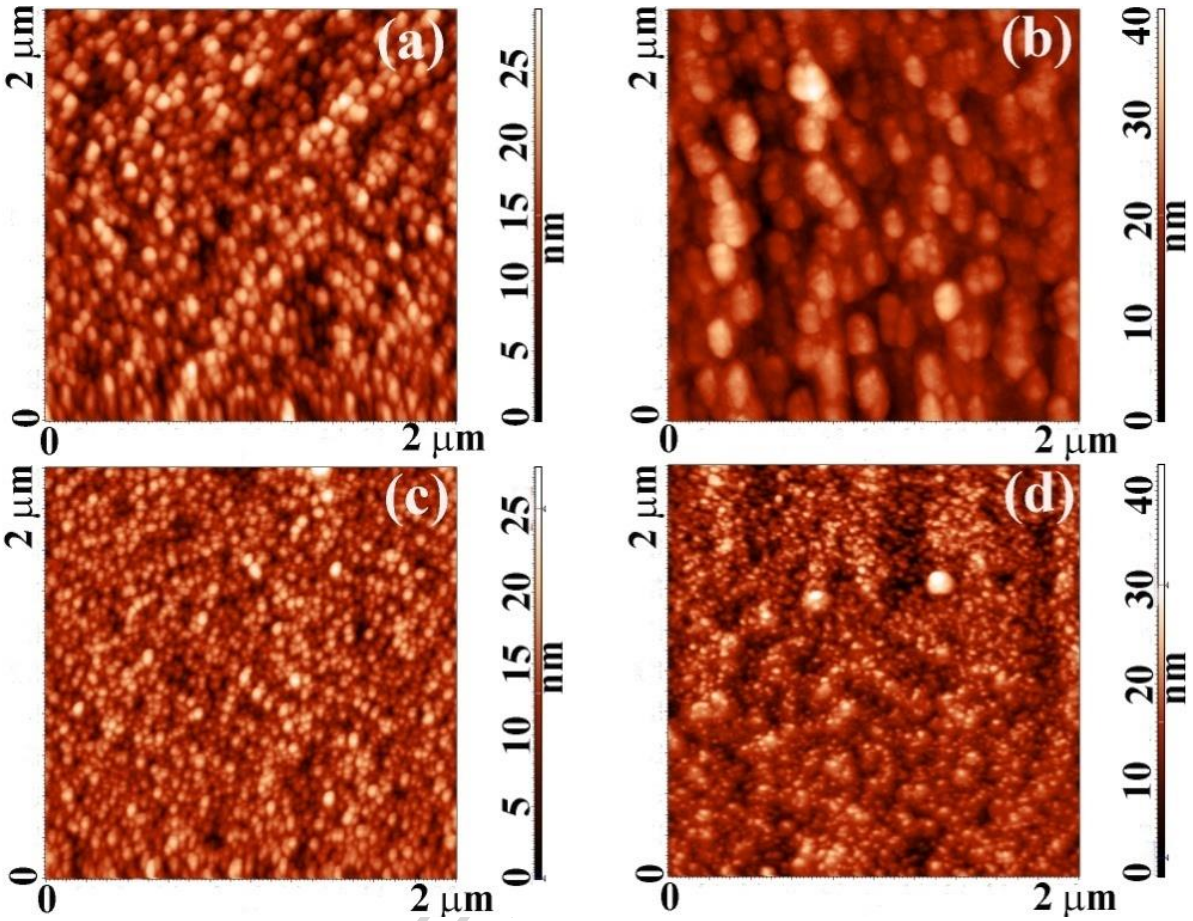

ACCEPTED

ACCEPTED MANUSCRIPT

Figure 6: Bright field transmission electron microscopy images of as-deposited and vacuum annealed Bi-rich Bi_2Te_3 films: (a) Bi-BT-AD, (b) Bi-BT-100, (c) Bi-BT-200 and (d) Bi-BT-300. Corresponding SAED patterns, (e) Bi-BT-AD, (f) Bi-BT-100, (g) Bi-BT-200 and (g) Bi-BT-300, are shown in right panel.

ACCEPTED MANUSCRIPT

ACCEPTED MANUSCRIPT

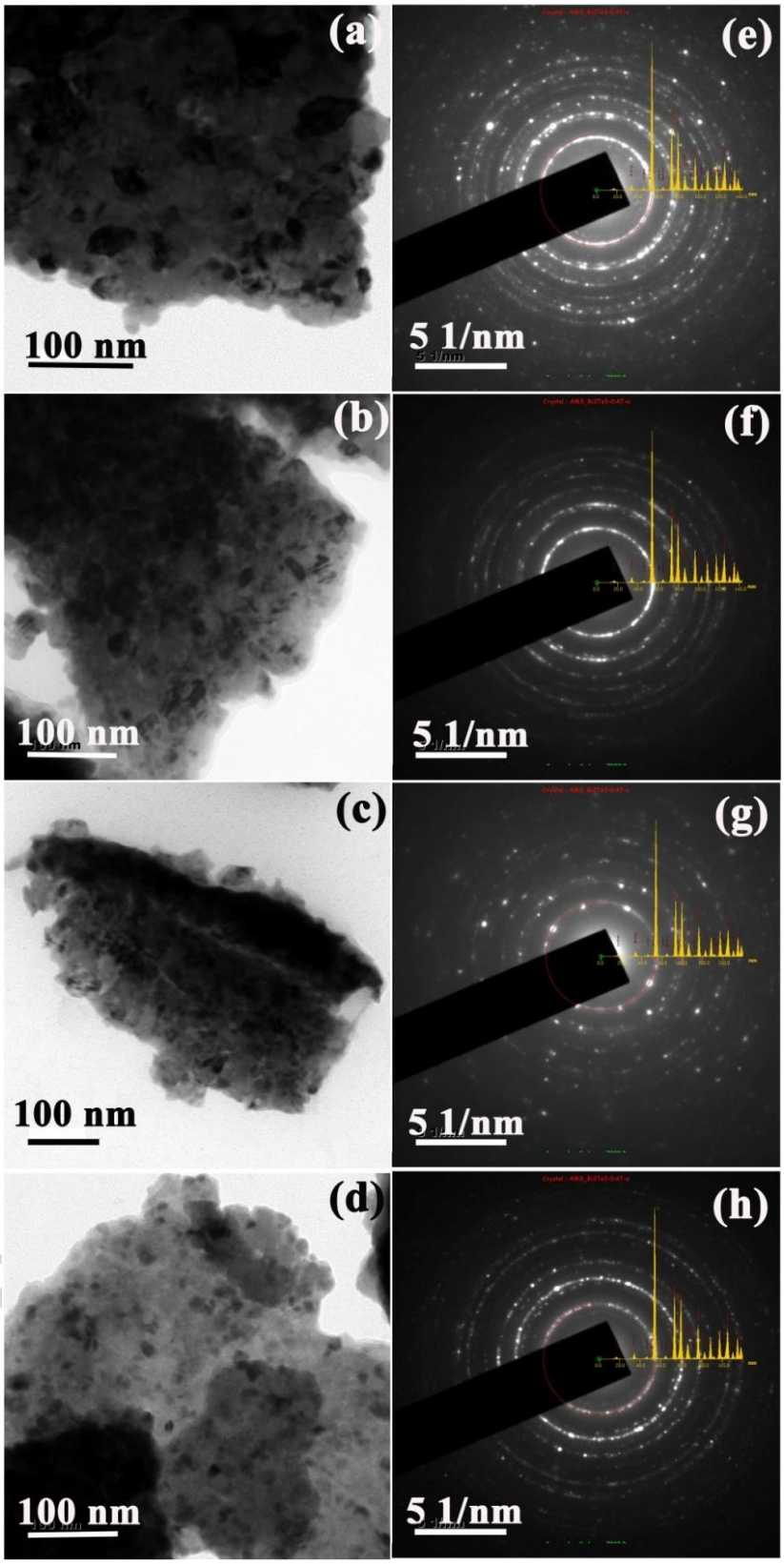

ACCEPTED MANUSCRIPT

Figure 7: High resolution transmission electron microscopy images of as-deposited and vacuum-annealed Bi-rich Bi_2Te_3 films. [(a) Bi-BT-AD, (b) Bi-BT-100, (c) Bi-BT-200 and (d) Bi-BT-300].

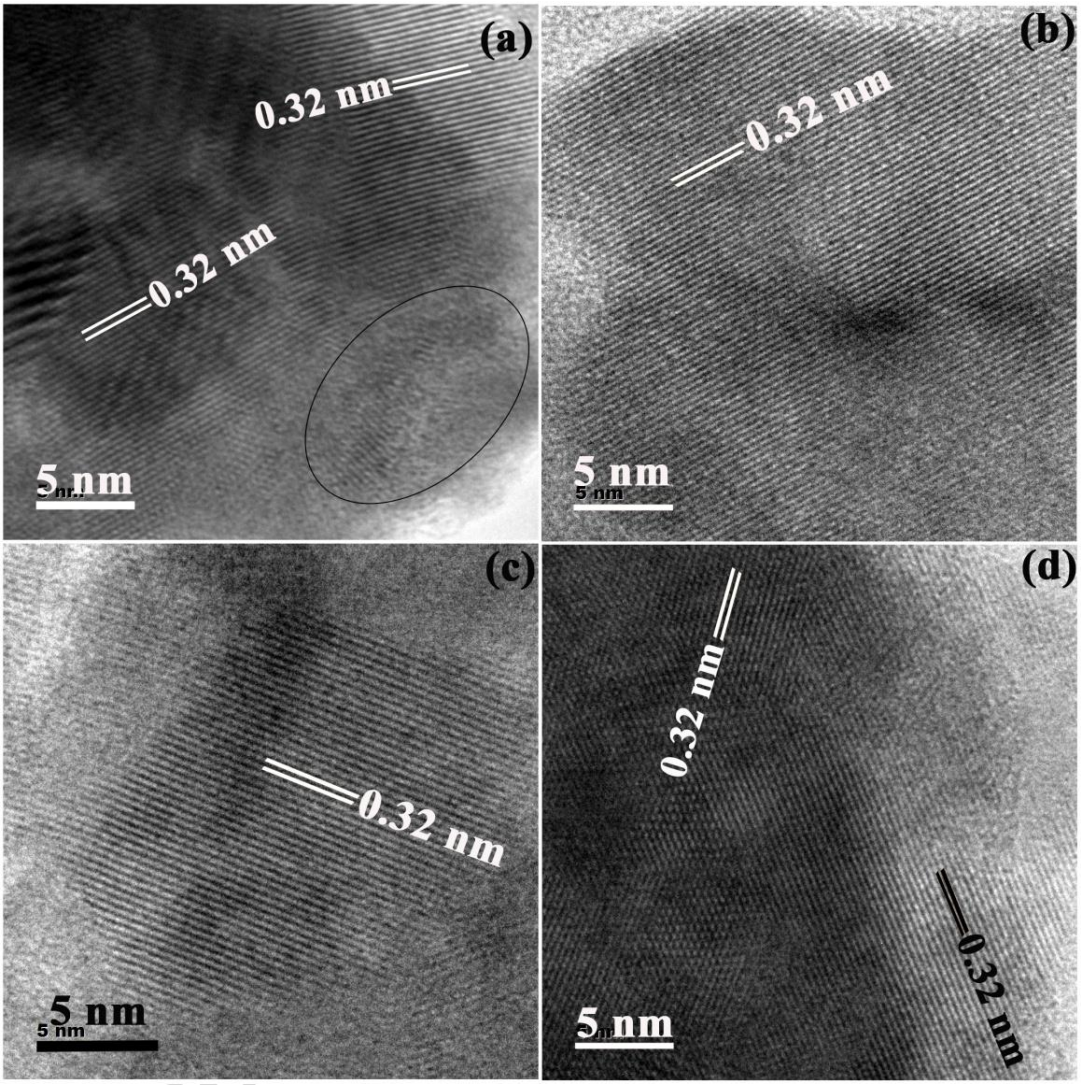

ACCEPTED MANUSCRIPT

Figure 8: (a) Diffuse Reflection spectra of as-deposited Bi-rich Bi_2Te_3 films and vacuum annealed at different temperatures. (b) and (c) show the K-M transformed reflectance spectra of as-deposited and vacuum annealed thin films for direct and indirect band, respectively.

ACCEPTED MANUSCRIPT

ACCEPTED MANUSCRIPT

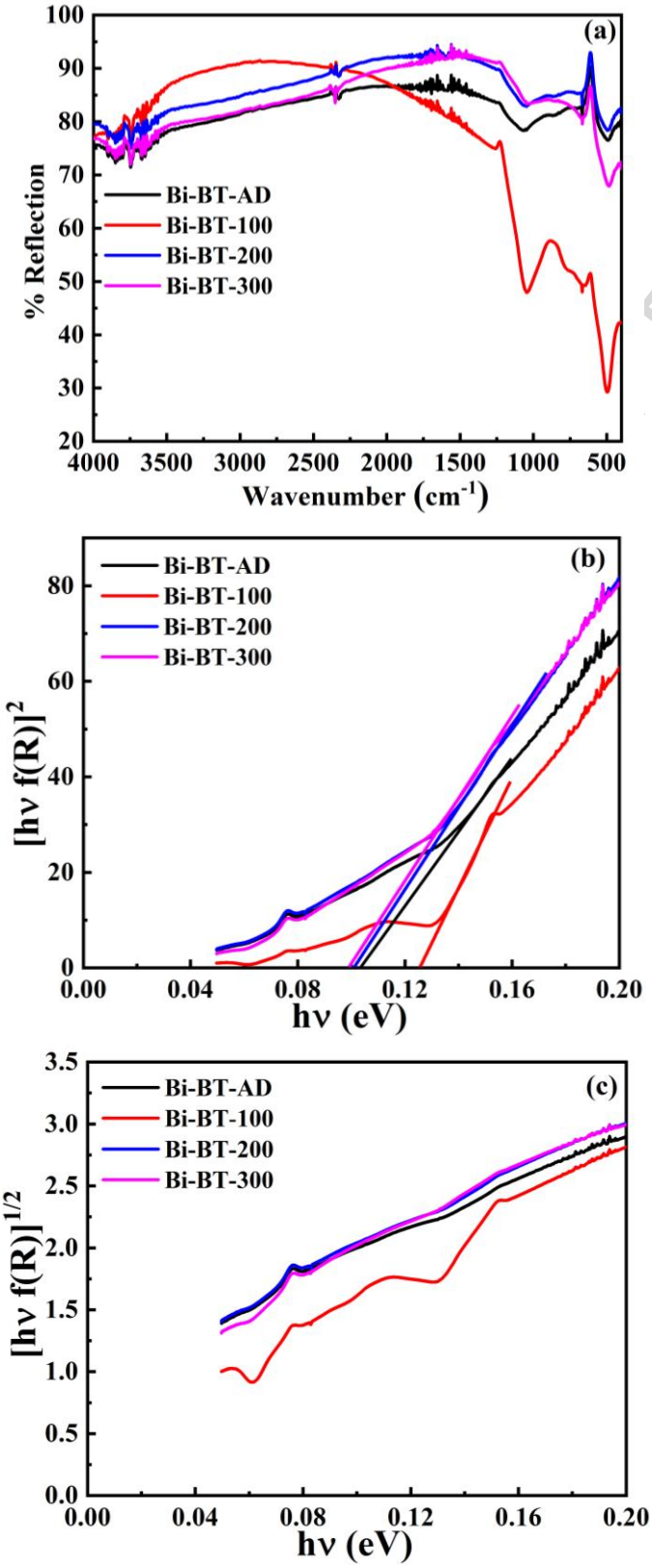

ACCEPTED MANUSCRIPT

Figure 9: Carrier density and mobility of as-deposited and vacuum annealed Bi–rich Bi_2Te_3 films.

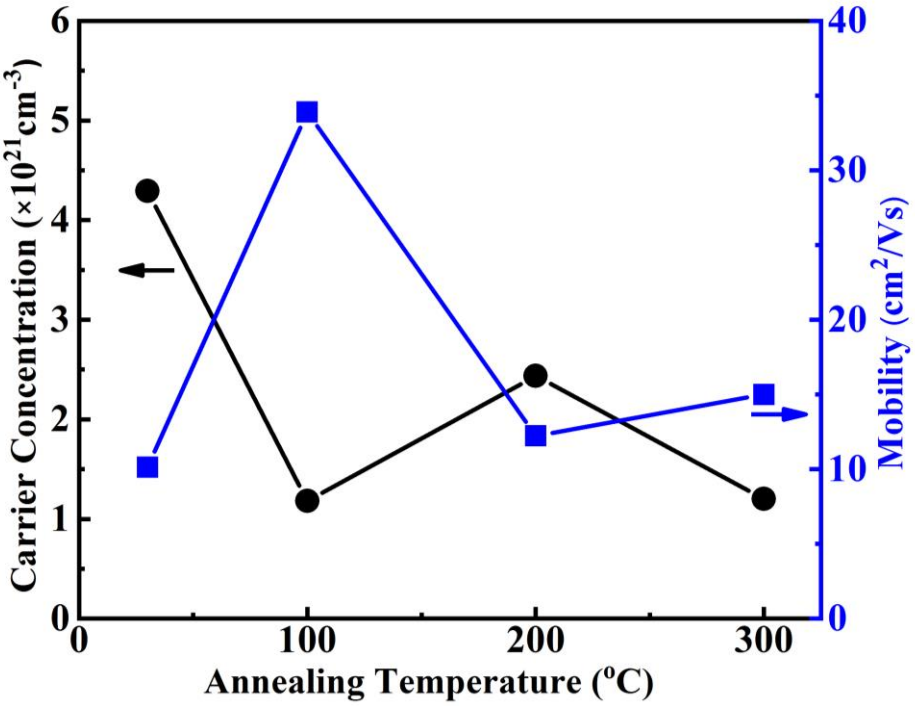

ACCEPTED MANUSCRIPT

ACCEPTED MANUSCRIPT

Figure 10: Temperature dependent resistivity of as-deposited and vacuum annealed Bi-rich Bi_2Te_3 films.

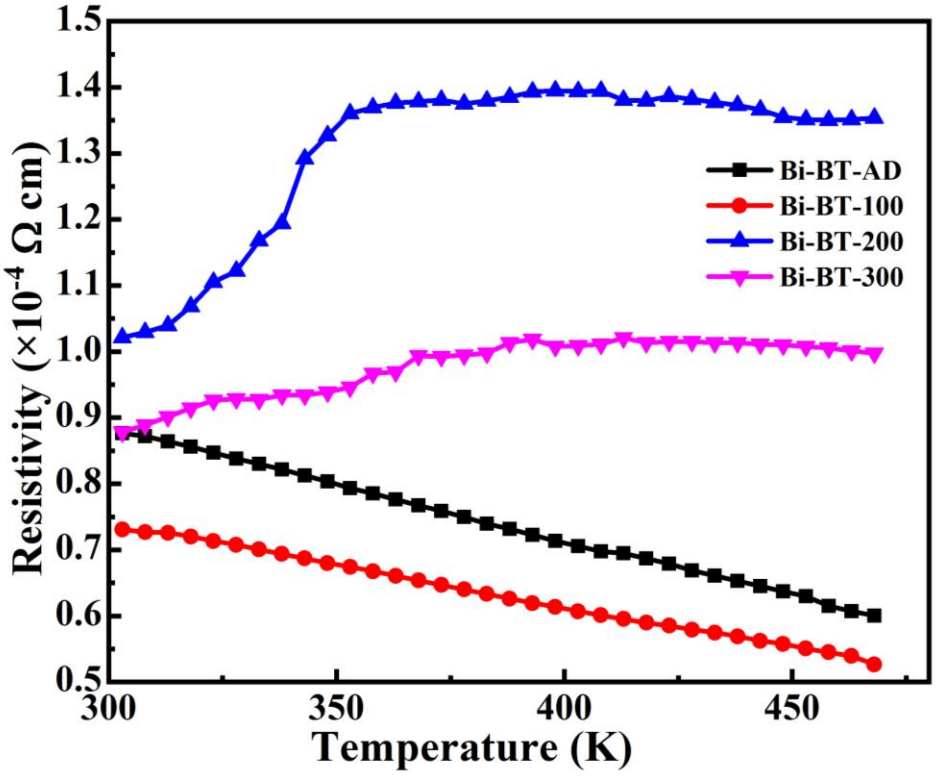

ACCEPTED MANUSCRIPT

Figure 11: Electrical and thermoelectric properties of as-deposited and vacuum-annealed Bi-rich Bi_2Te_3 films measured at room temperature.

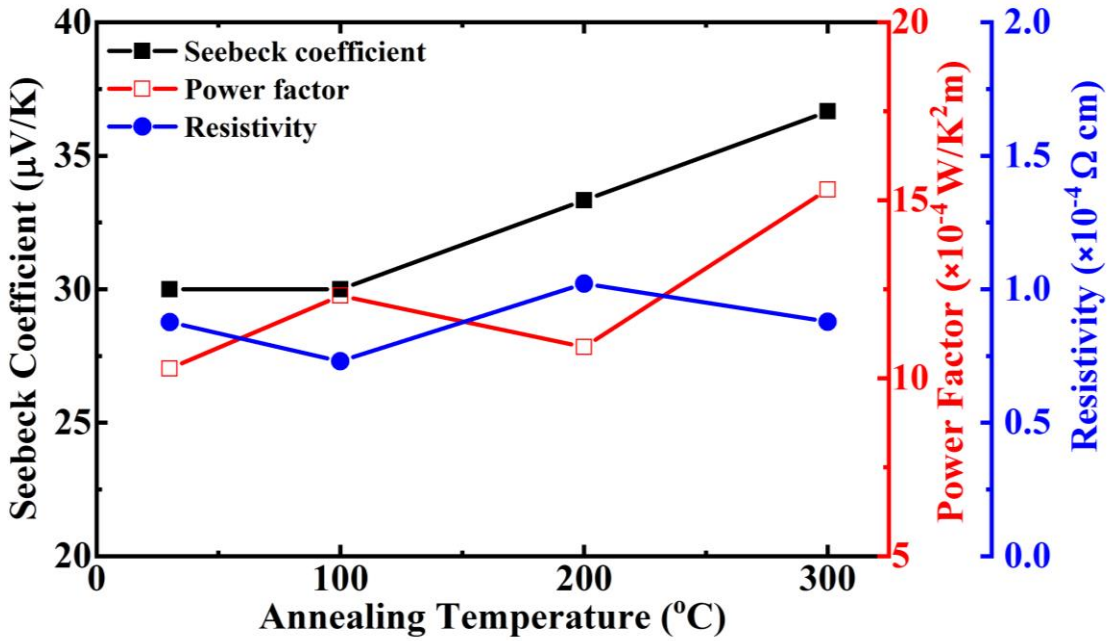

ACCEPTED MANUSCRIPT

Figure 12: (a) The effect of applied temperature on Seebeck coefficient of as-deposited and vacuum annealed Bi-rich Bi_2Te_3 films. (b) The effect of applied temperature on power factor of Bi-rich Bi_2Te_3 films.

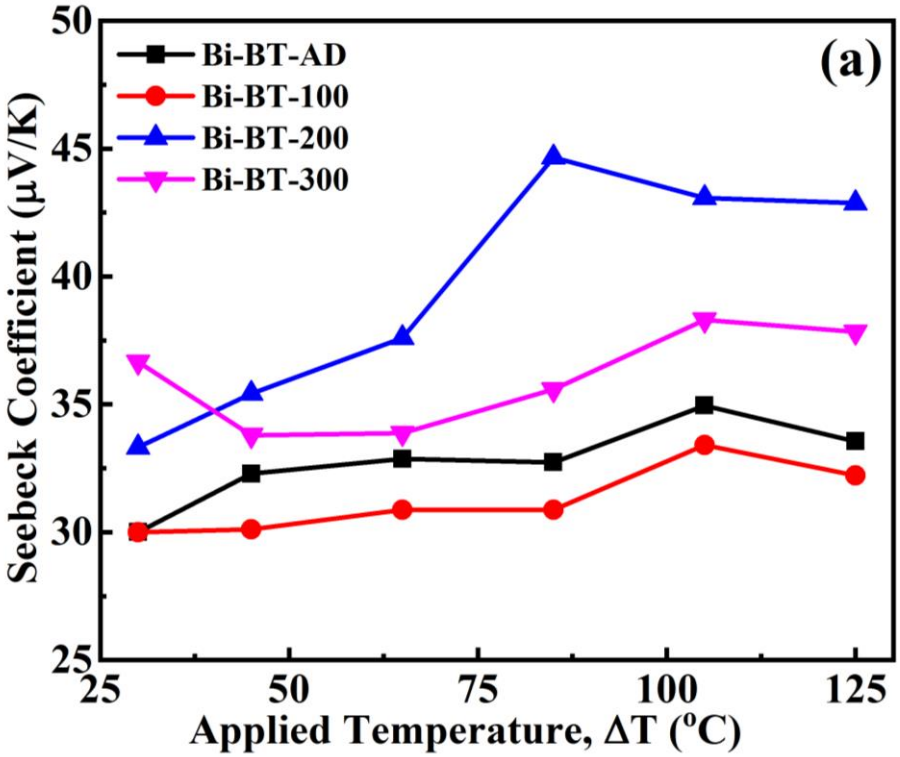

ACCEPTED MANUSCRIPT

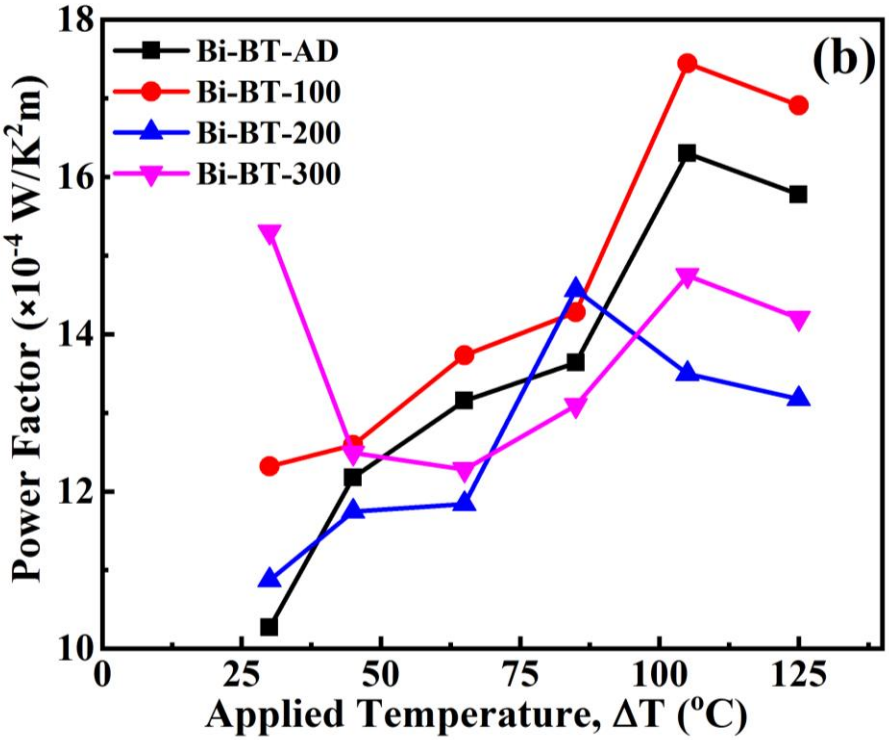

Figure 13: The effect of vacuum annealing temperature on (a) resistivity, (b) Seebeck coefficient and (c) power factor of near stoichiometric Bi_2Te_3, Te-rich Bi_2Te_3 and Bi-rich Bi_2Te_3 films measured at room temperature.

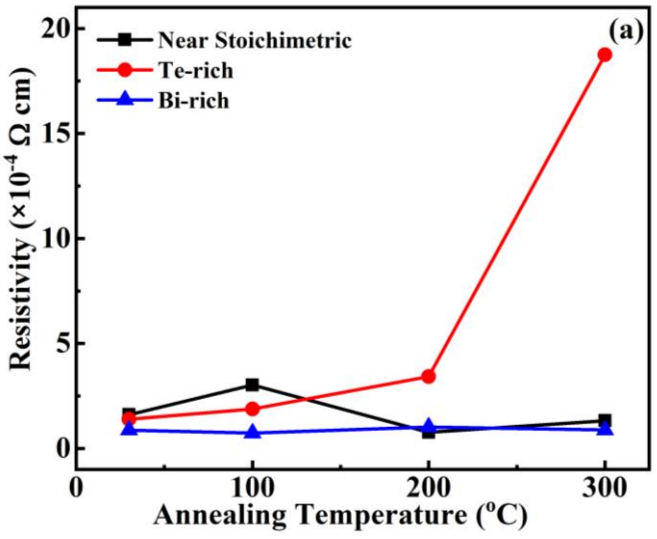

ACCEPTED MANUSCRIPT

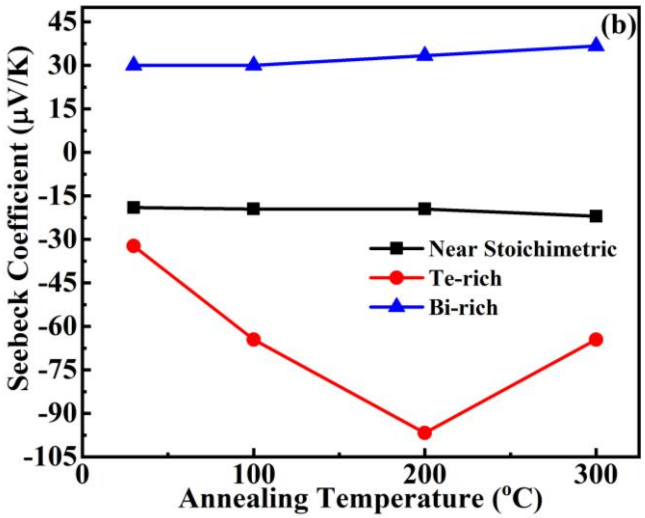

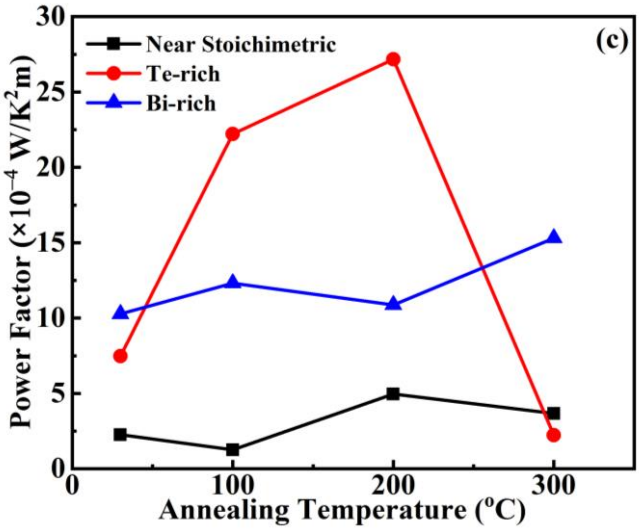

ACCEPTED MANUSCRIPT

Highlights

- Nanocrystalline Bi-rich Bi_2Te_3 (Bi-BT) thin films are made by e-beam evaporation
- Vacuum annealed Bi-BT thin films exhibit p-type conductivity
- High power factor of ~ 17.5×10^{-4} W/K^2m are favorable for thermoelectric applications
- For low temperature processed device applications, Bi-BT are most suitable.
- Bi-BT require low annealing (~100 °C) to acquire desirable thermoelectric properties

ACCEPTED MANUSCRIPT